Article

The hysteresis of the Antarctic Ice Sheet

https://doi.org/10.1038/s41586-020-2727-5

Received: 5 April 2019

Accepted: 11 August 2020

Published online: 23 September 2020

Check for updates

Julius Garbe[1,2], Torsten Albrecht[1], Anders Levermann[1,2,3], Jonathan F. Donges[1,4] & Ricarda Winkelmann[1,2]✉

More than half of Earth's freshwater resources are held by the Antarctic Ice Sheet, which thus represents by far the largest potential source for global sea-level rise under future warming conditions[1]. Its long-term stability determines the fate of our coastal cities and cultural heritage. Feedbacks between ice, atmosphere, ocean, and the solid Earth give rise to potential nonlinearities in its response to temperature changes. So far, we are lacking a comprehensive stability analysis of the Antarctic Ice Sheet for different amounts of global warming. Here we show that the Antarctic Ice Sheet exhibits a multitude of temperature thresholds beyond which ice loss is irreversible. Consistent with palaeodata[2] we find, using the Parallel Ice Sheet Model[3–5], that at global warming levels around 2 degrees Celsius above pre-industrial levels, West Antarctica is committed to long-term partial collapse owing to the marine ice-sheet instability. Between 6 and 9 degrees of warming above pre-industrial levels, the loss of more than 70 per cent of the present-day ice volume is triggered, mainly caused by the surface elevation feedback. At more than 10 degrees of warming above pre-industrial levels, Antarctica is committed to become virtually ice-free. The ice sheet's temperature sensitivity is 1.3 metres of sea-level equivalent per degree of warming up to 2 degrees above pre-industrial levels, almost doubling to 2.4 metres per degree of warming between 2 and 6 degrees and increasing to about 10 metres per degree of warming between 6 and 9 degrees. Each of these thresholds gives rise to hysteresis behaviour: that is, the currently observed ice-sheet configuration is not regained even if temperatures are reversed to present-day levels. In particular, the West Antarctic Ice Sheet does not regrow to its modern extent until temperatures are at least one degree Celsius lower than pre-industrial levels. Our results show that if the Paris Agreement is not met, Antarctica's long-term sea-level contribution will dramatically increase and exceed that of all other sources.

The Antarctic Ice Sheet comprises an ice mass equivalent to 58 m of global sea-level rise[1]. Its future evolution and the associated sea-level change are therefore of profound importance to coastal populations, ecosystems and economies. Over the past decades, the ice sheet has been losing mass at an accelerating rate[6,7]. Although the current net mass loss from Antarctica is small compared to the other sea-level rise contributions, it is likely to increase with progressing global warming[8]. Snowfall can be expected to increase in a warming atmosphere[9], but this additional accumulation is likely to be counteracted and eventually overcompensated by ice dynamical effects[10].

The long-term stability of the Antarctic Ice Sheet under a changing climate is the subject of ongoing research. It will be determined by the interplay between a number of negative (dampening) and positive (amplifying) feedbacks[8]. The latter might eventually lead to the crossing of critical thresholds, with the ice sheet entering into an irreversible dynamic, committing it to a specific amount of sea-level contribution.

One such self-amplifying feedback is the so-called surface-melt–elevation feedback. Whereas at present in Antarctica there is very little surface melt, it might increase with strong global warming. The resulting lowered surface elevation exposes the ice to warmer temperatures through the atmospheric lapse rate, in turn leading to more melting[11–14]. Once a critical temperature threshold is crossed, this melt-induced lowering of the ice-sheet surface elevation can trigger accelerated ice loss. In addition, the ice flow is generally accelerated under warmer temperatures, as viscosity decreases and deformation rates for a given stress increase. Through enhanced strain heating, this effect facilitates basal sliding and sped-up ice stream flow and might eventually result in a runaway process known as "creep instability"[15].

Regions of the ice sheet that rest on bedrock below sea level are prone to additional feedback mechanisms, which can potentially drive the collapse of Antarctic Ice Sheet basins. Such regions—termed marine ice-sheet regions—can be found in most of West Antarctica as well as in substantial parts of East Antarctica (for example, the Aurora and Wilkes subglacial basins). One self-reinforcing feedback mechanism associated with these regions is the marine ice-sheet instability, which implies a potential for irreversible grounding-line retreat on retrograde

[1]Potsdam Institute for Climate Impact Research (PIK), Member of the Leibniz Association, Potsdam, Germany. [2]Institute of Physics and Astronomy, University of Potsdam, Potsdam, Germany. [3]Lamont-Doherty Earth Observatory, Columbia University, New York, NY, USA. [4]Stockholm Resilience Centre, Stockholm University, Stockholm, Sweden. ✉e-mail: ricarda.winkelmann@pik-potsdam.de

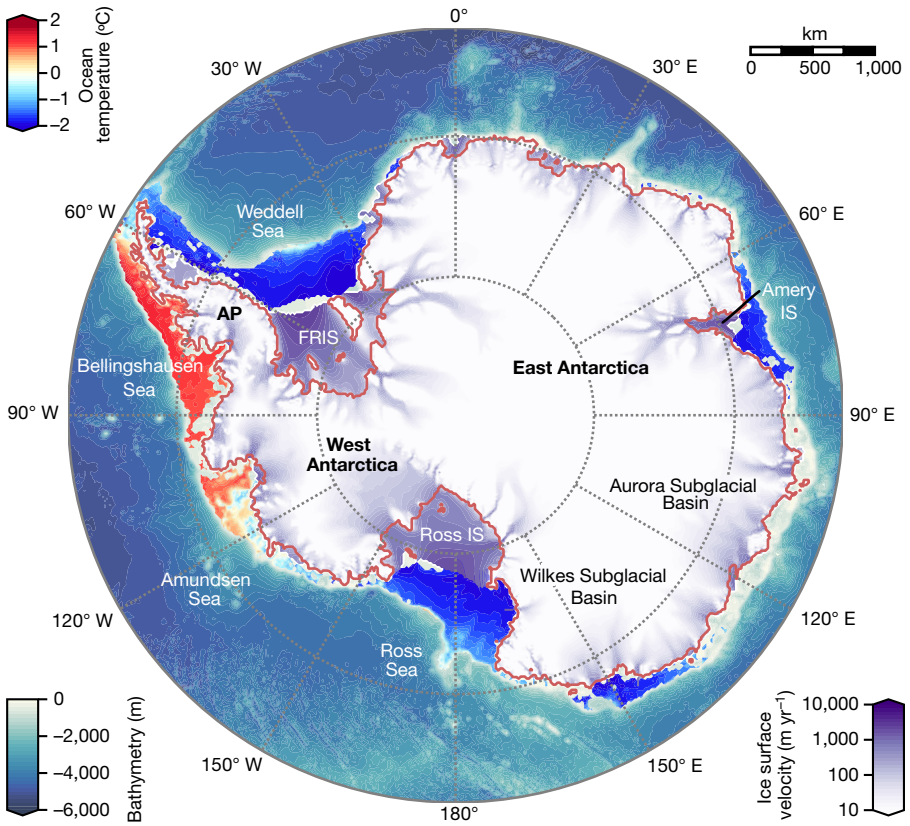

Fig. 1 | Antarctic ice velocities and surrounding ocean temperatures. Simulated ice surface velocities (in metres per year) of the reference ice-sheet state revealing the fast-flowing ice streams (purple shadings). Ocean temperatures at continental shelf depth (blue–red shading) are from ref. [38]. The simulated grounding-line locations are shown in red. AP, Antarctic Peninsula; IS, ice shelf; FRIS, Filchner–Ronne Ice Shelf.

sloping bedrock[8,16,17]. However, in the presence of sufficiently large ice-shelf buttressing, grounding lines on retrograde bed slopes can be conditionally stable[18].

A potential negative feedback is introduced by solid-Earth rebound: marine ice-sheet mass loss leads to a drop in sea level at the grounding line as a response to post-glacial rebound of the unloaded crust. This can effectively reduce the ice outflow, thereby acting as a stabilizing mechanism[19].

There are several further positive and negative feedback mechanisms caused by the interaction of the Antarctic Ice Sheet with the surrounding ocean, sea ice, atmosphere and the solid Earth[20]. These, however, are not included in the analysis presented here because, as discussed below, they either require a deeper understanding or they can be expected to have a less substantial impact on the long-term stability of the ice sheet.

Here we investigate the long-term response of the Antarctic Ice Sheet to various levels of warming with the fully dynamic Parallel Ice Sheet Model (PISM[3–5]). Owing to the interplay between the dampening and amplifying feedbacks, the response of the Antarctic ice volume to temperature change is expected to be highly nonlinear, and critical threshold behaviour might occur[21,22], leading to committed sea-level contribution upon transgression. This implies the existence of a hysteresis, that is, a path-dependent difference between multiple stable ice-sheet states, similar to what has been shown for the Greenland Ice Sheet[23]. As yet, however, large uncertainties remain concerning the warming levels at which these thresholds are reached and which regions of Antarctica could undergo irreversible ice loss under future warming[21,24–28].

In an earlier study[24] focusing on the terrestrial parts of the Antarctic Ice Sheet, a step-warming approach was used to localize the critical thresholds leading to large-scale retreat of the West and East Antarctic ice sheets at regional surface air temperature anomalies of about 8 °C and 16 °C, respectively. However, the applied model did not account for any ice–ocean interactions, which means that ice-sheet retreat is driven purely by surface mass balance processes and therefore the warming required to destabilize the marine regions of the West Antarctic Ice Sheet is likely to be overestimated.

From palaeorecords and modelling studies, we know that rapid transitions of the order of one to several thousand years between glacial, intermediate and collapsed states for West Antarctica are possible[29–31], and hysteresis effects might have occurred in the Cenozoic era[32,33]. During the global climatic shift towards colder temperatures near the Eocene–Oligocene boundary around 34 million years ago, which set off the sudden, widespread glaciation of Antarctica[34], globally averaged surface temperatures have cooled by about 4–5 °C (ref. [35]). Owing to human action, the Earth system is currently on a trajectory towards a reversal of this major transition, which emphasizes the urgency of adhering to the Paris Agreement's target of limiting global warming to well below 2 °C above pre-industrial temperatures in order to avoid the crossing of critical thresholds, committing us to long-term and possibly irreversible sea-level rise.

Long-term stability simulations

To study the future long-term response of the Antarctic Ice Sheet to changing global temperatures, we trace the ice sheet's hysteresis using a technique that is routinely used to analyse, for instance, the stability of the Atlantic meridional overturning circulation and other climate components, as described in detail in section 2b of ref. [36]: the global mean temperature (GMT), which we define here as the globally averaged surface air temperatures over land and ocean, is converted into regional changes of surface air and ocean temperature and ramped up

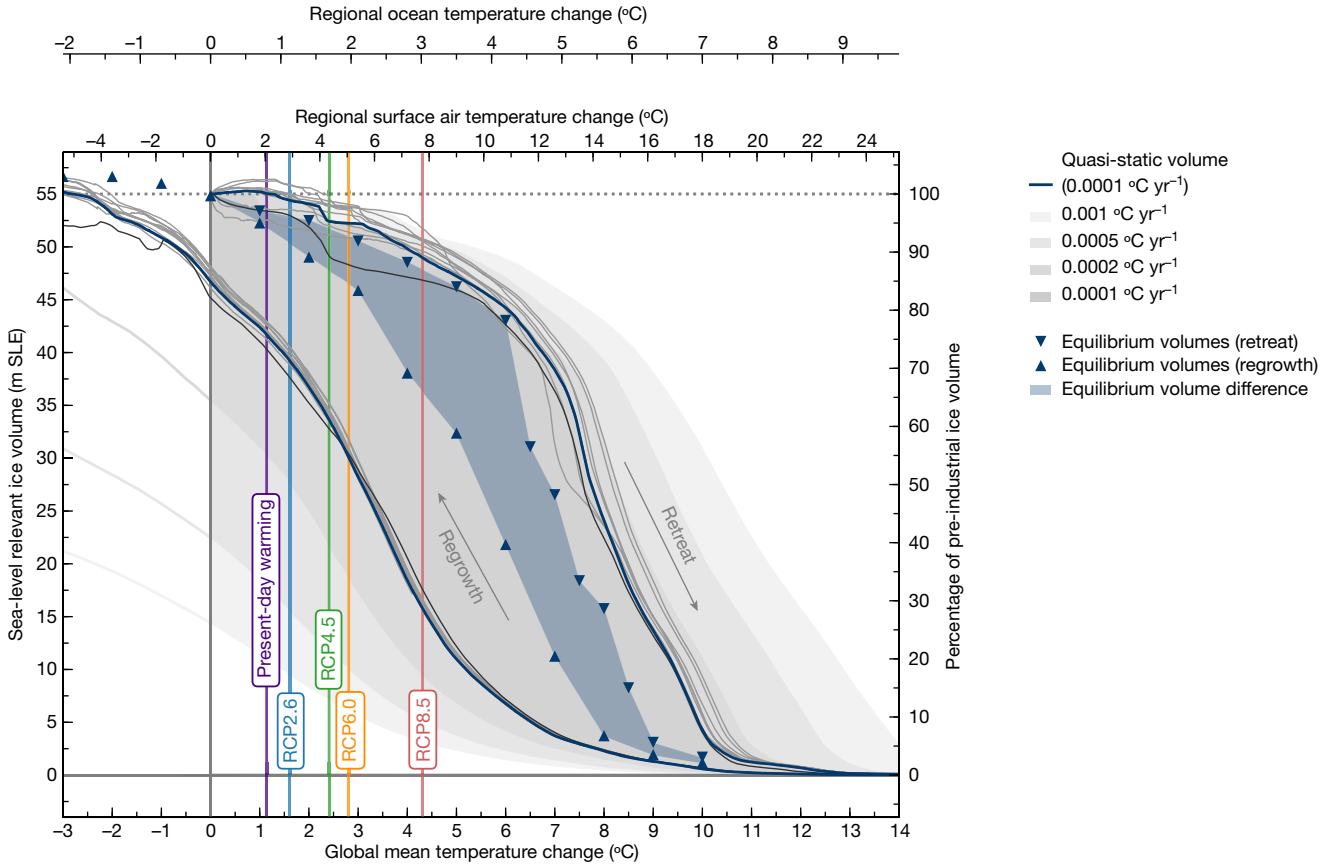

Fig. 2 | Hysteresis of the Antarctic Ice Sheet. Sea-level relevant ice volume (in metres sea-level equivalent, m SLE) for the quasi-static reference simulations (blue curve) as well as the corresponding equilibrium states at discrete temperature levels (blue triangles). The blue filled area marks the hysteresis gap, that is, the equilibrium volume difference between the upper and lower hysteresis branches. Grey shadings correspond to different rates of applied GMT change. The quasi-static simulations based on an ensemble of perturbed model parameters are given as thin light grey lines and are shown in more detail in Extended Data Fig. 4. The dark grey line denotes the quasi-static simulation using a model grid resolution of 8 km. Vertical coloured bars mark the GMT levels of present-day observed warming as well as expected end-of-century warming levels for the four different RCP scenarios[8].

incrementally until complete deglaciation is reached (for details, see Methods). The applied rate of GMT change is slower than the typical response timescale of the ice sheet and is chosen in such a way that the system can follow the change while remaining as close as possible to equilibrium at all times. Advantages of this method compared to step-like temperature changes are that it avoids any abrupt overshoot effects and allows a continuous disentanglement of the relevant mass balance processes over the entire temperature range. Ideally, the branches of the hysteresis would be determined by an infinitely slow temperature change. Since available computational resources pose a constraint on the lower limit of this rate, we approximate this ideal case by applying the slowest computationally feasible rate of GMT change of 0.0001 °C yr^{-1} in a quasi-static reference simulation (hereafter referred to as 'quasi-static' simulations) and investigate the influence of faster rates on the ice sheet's response by varying the applied rate between 0.0001 °C yr^{-1} and 0.001 °C yr^{-1}. The quasi-static simulations are further extended at fixed temperature levels (at every full degree, as well as every half degree between 6 °C and 9 °C above pre-industrial temperatures during ice-sheet retreat) until the ice sheet fully reaches a steady state, that is, volume changes become negligible (hereafter referred to as 'equilibrium' simulations). To investigate the ice sheet's ability to regrow after complete disintegration, we reverse the temperature anomaly at the same rate (that is, −0.0001 °C yr^{-1} in the quasi-static reference case).

Our simulations are initialized from a reference equilibrium state that resembles the pre-industrial Antarctic Ice Sheet geometry as closely as possible while adequately approximating observed ice velocities at the same time (see Methods and Extended Data Figs 1 and 2). We specifically aim for a good representation of the ice-sheet geometry in steady state, because starting from steady state is required for a systematic realization of the hysteresis methodology as described above. In a different study[37] we have shown that our model is also capable of adequately reproducing Antarctica's evolution over the last two glacial cycles. Surface speeds range over more than five orders of magnitude from merely centimetres per year in the ice sheet's interior to several kilometres per year in the ice streams and ice shelves (Fig. 1).

Most of the ice sheet is surrounded by ocean waters with temperatures below zero. However, ice shelves in the Amundsen and Bellingshausen seas are in contact with relatively warm ocean waters of temperature up to 1.8 °C at the depth of the continental shelf region[38]. Recent observations show that the glaciers, especially in the Amundsen region, have accelerated notably over the past decades[39,40] and that a marine ice-sheet collapse might already be under way in this sector[41,42].

Ice-sheet hysteresis

The equilibrium response of the Antarctic Ice Sheet reveals a strong hysteresis behaviour over the entire range of global warming up to around 10 °C above pre-industrial temperatures (Fig. 2, blue-shaded area and triangle markers). Above these warming levels, Antarctica would eventually become virtually ice-free. Palaeoevidence suggests that this has not been the case since around 34 million years ago[34], when global mean surface temperatures were around 6–8 °C warmer compared to the pre-industrial average[35].

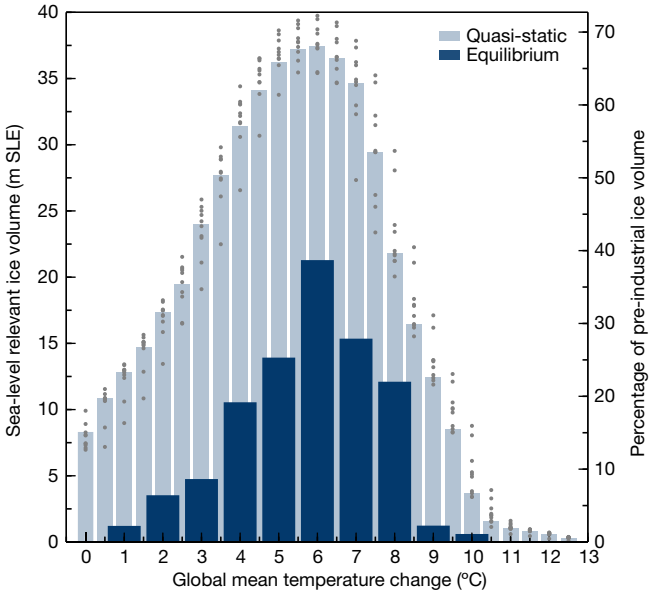

Fig. 3 | Ice-sheet volume differences between retreat and regrowth. The bar charts show the ice volume differences (in m SLE) between the retreat and regrowth branches of the hysteresis curve for discrete warming levels. Light blue bars are based on the quasi-static simulations (blue lines in Fig. 2), dark blue bars on the equilibrium states (blue triangle markers in Fig. 2). Grey dots denote the uncertainty range for the quasi-static simulations (full ensemble spread of all tested model parameters, as detailed in Extended Data Fig. 4).

The rates of ice-sheet retreat and regrowth, that is, the ice sheet's sensitivity to the external forcing, generally depend on the magnitude of the applied rate of GMT change (Fig. 2, grey shadings), with smaller forcing rates resulting in stronger retreat and regrowth. The quasi-static simulations (Fig. 2, blue curves) thereby approximate the equilibrium volumes (the 'true' hysteresis) most closely, as expected.

The decline of the ice sheet occurs in several disjunct stages. Initially, below 1 °C of warming, the ice volume in the quasi-static simulation in fact increases slightly owing to the effect of additional snowfall[9], especially in East Antarctica. The influence of enhanced snowfall is, however, minor compared to the overall mass losses of Antarctica in response to warmer temperatures. At warming levels between 1 °C and 2.5 °C, grounding lines in West Antarctica start strongly retreating (Supplementary Video 1), resulting in mass losses equivalent to more than 2 m of sea-level rise in equilibrium and even exceeding that value in the quasi-static simulation (that is, at a warming rate of 0.0001 °C yr^{-1}). The quasi-static curve up to 4 °C of warming as obtained here is consistent with Antarctic palaeodata from the past five million years[43] as well as corresponding simulations with a different ice-sheet model[29] as shown in ref. [44].

Between 6 °C to 9 °C above pre-industrial temperatures a second major threshold is found, manifesting in a loss of more than 70% of the total ice mass upon transgression, corresponding to long-term global sea-level rise of more than 40 m SLE (metres sea-level equivalent; only accounting for ice volume above flotation, hereafter referred to as 'sea-level relevant ice volume').

For some warming levels, equilibrium and quasi-static sea-level relevant ice volumes differ substantially, suggesting that the crossing of a threshold caused the system to diverge from its stable evolutionary path. Hence, it can be assumed that the critical temperature at which a large-scale decline of ice-sheet sectors is induced is therefore effectively lower than it appears in the quasi-static simulations. In particular, while ice-sheet sectors in West Antarctica seem to be still largely intact at 1–2 °C of warming in the quasi-static simulations, the equilibrium response shows that even below this temperature level, major portions of the marine regions of the West Antarctic Ice Sheet are already committed to long-term collapse (compare quasi-static ice-sheet evolution shown in Supplementary Video 1 and equilibrium ice-sheet responses shown below), which is consistent with earlier results[27]. Similar discrepancies in quasi-static and equilibrium ice loss can be seen at temperatures around 6–7 °C, associated with the collapse of major basins in East Antarctica.

The ice-sheet volume follows two substantially different paths during retreat and regrowth (see the lower set of branches in Fig. 2 and Supplementary Video 2). At pre-industrial temperatures, the modelled ice sheet regains almost its original sea-level relevant ice volume in equilibrium. However, the spatial ice-thickness distribution varies strongly from the starting configuration (Extended Data Fig. 3). In particular, West Antarctic grounding lines do not re-advance to their present-day locations until temperatures are at least 1 °C lower than pre-industrial levels. In the quasi-static simulations, the sea-level relevant ice volume deviates from the initial value by more than 8 m SLE at pre-industrial temperatures. The original volume is only regained at around 3 °C lower than pre-industrial temperatures. Around 4 °C lower than pre-industrial temperatures, the grounding lines in most regions re-advance close to their original position. This suggests that the present-day configuration of the Antarctic Ice Sheet might indeed be a legacy of the last ice age, when temperatures were about 3–4 °C lower than today's.

The sizable gap between the upper and lower branches of the hysteresis diagram shows that Antarctic ice-sheet retreat is to a great extent irreversible. The difference between the retreat and regrowth ice volumes is largest at around 6 °C of warming, reaching more than 20 m SLE in equilibrium and even more than 35 m SLE in the quasi-static simulations (Fig. 3). The discrepancy between the quasi-static and equilibrium volume responses is even larger for the regrowth path, mainly owing to the longer timescales associated with the build-up of the ice-sheet.

The ice-sheet response and general behaviour is robust with respect to changes in model resolution, ice-shelf calving, mantle response to ice loading, ice-stream sliding, and ice-flow enhancement factors. This applies in particular to the overall results for warming levels exceeding approximately 8 °C (Extended Data Fig. 4). Our sensitivity tests reveal an average uncertainty spread of around 5.5 m SLE for the tested range of parameter values, mainly originating from the retreat branch and the steepness of the hysteresis curve between 6 °C and 9 °C of warming. The uncertainty at temperatures below about 5 °C of warming is dominated by model resolution and the ice-flow enhancement factor, whereas at temperatures between 6 °C and 8 °C it is dominated by the sliding factor and mantle response, peaking at about 12 m SLE at around 7–8 °C of warming, when the second major threshold is passed. The exact temperature threshold of marine ice-sheet instabilities in West Antarctica and the Wilkes subglacial basin are highly sensitive to model parameters and resolution, highlighting the particularly low resilience of the system in this temperature range; the respective thresholds need to be constrained further in a per-basin approach.

Figure 4 compares the ice-sheet equilibrium configurations during retreat and regrowth at different levels of warming. At 1 °C of warming, the Filchner–Ronne Ice Shelf is still largely intact following the retreat path, whereas it fails to regrow at the same temperature level on the regrowth path. At a warming level of 2 °C, various parts of the East Antarctic Ice Sheet that are still present at this temperature during retreat do not fully re-advance during regrowth, as, for instance, in the Wilkes subglacial basin. This is consistent with earlier studies that have found that Wilkes basin is currently protected by a small ice plug, but that large-scale, irreversible retreat can occur once this ice plug is removed[45,46]. This difference is even more pronounced at 4 °C of warming, for which additionally major parts of the Aurora subglacial basin are still ice-free during regrowth. For temperatures between 6 °C and 8 °C, the difference is most prominent, with ice margins almost nowhere reaching their corresponding extent during the regrowth (see also

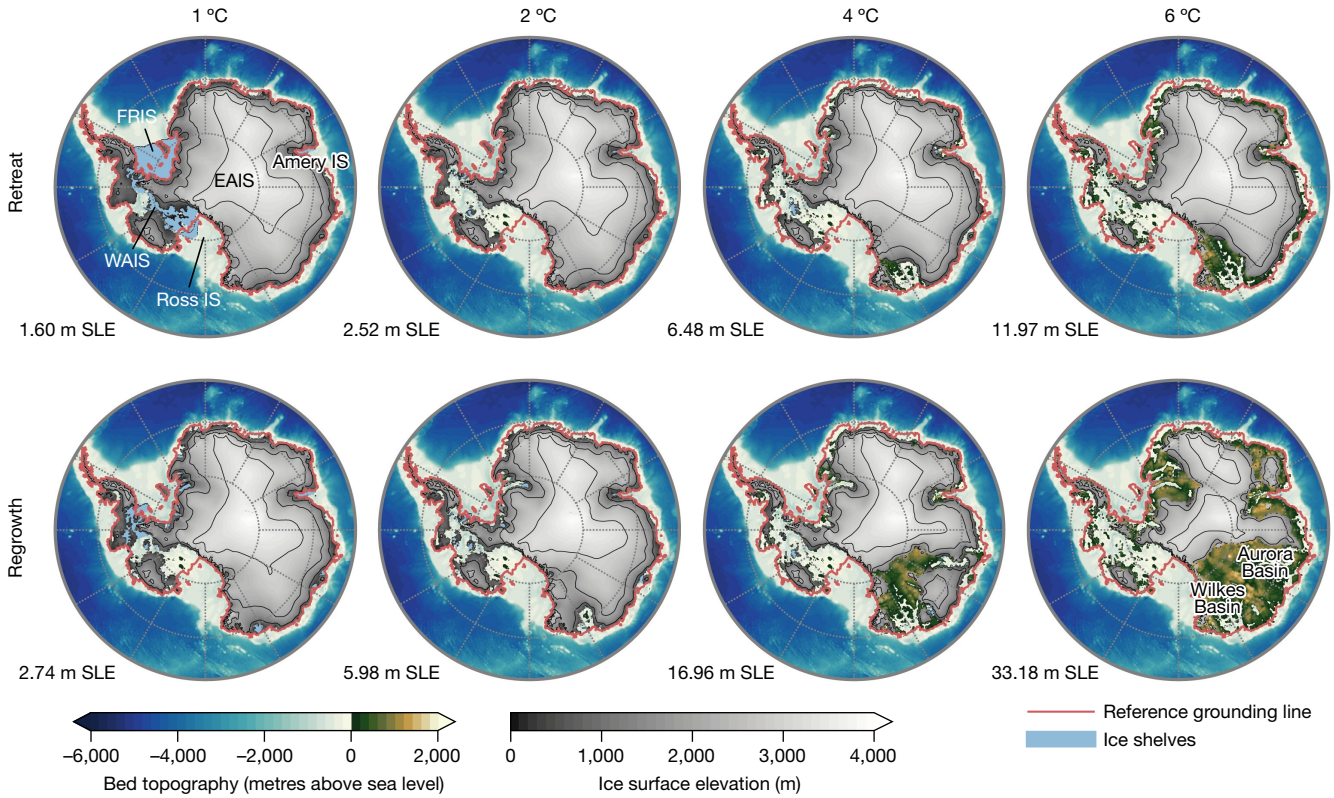

Fig. 4 | Long-term ice loss for different warming levels. The equilibrium ice-sheet surface elevation is shown in metres for different warming levels (1 °C, 2 °C, 4 °C and 6 °C GMT anomaly above pre-industrial level), comparing the retreat (upper panels) and regrowth (lower panels) branch of the hysteresis curve. Ice surface-height contours are delineated at 1,000-m intervals. Grounding-line locations of the reference state are shown in red; ice shelves are marked in light blue. The absolute sea-level relevant ice-volume anomaly compared to the reference state (in m SLE), that is, the committed sea-level rise, is given for each panel. Blue shadings illustrate the bedrock depth in metres below the present-day sea level; brown shadings illustrate the bedrock elevation in metres above the present-day sea level. EAIS, East Antarctic Ice Sheet; WAIS, West Antarctic Ice Sheet. See Extended Data Fig. 5 for a continuation of this figure.

Extended Data Fig. 5). At even higher warming levels, the differences between retreat and regrowth lessen again, when smaller ice caps can only exist at some high-altitude locations.

Ocean-induced versus atmosphere-induced changes

Disentangling the different relevant mass balance processes for the upper hysteresis branch reveals the distinct nature of the two major thresholds (Fig. 5): The collapse of the West Antarctic Ice Sheet at around 2 °C of warming is driven mainly by increased sub-shelf melting and dynamic discharge (seen as a major peak in the basal mass balance flux). This process is also associated with substantial grounding-line retreat and the subsequent formation of extensive shelf areas, hinting at an active marine ice-sheet instability (Supplementary Video 1). At around 7 °C of warming, the overall surface mass balance turns negative. At these temperatures, the ice sheet has only very little contact with the ocean left. Consequently, in contrast to the first threshold, the strong decline of the East Antarctic Ice Sheet initiated at around 6–7 °C of warming is dominated by the surface elevation feedback, resulting in a steep lowering of the ice sheet's surface altitude and reduction of its area (seen as a sharp drop in surface mass balance flux; see also Supplementary Video 1).

A similar split-up of the lower hysteresis branch confirms that certain processes are dominant for given temperature regimes (Extended Data Fig. 6). The regrowth of the ice sheet is generally dominated by surface mass balance processes. Mass loss from basal melt is highest around 1 °C of warming, whereas in the retreat case the maximum mass loss occurs around 2 °C of warming. Interestingly, the surface mass balance flux reaches a similar value at 0 °C GMT anomaly during both the retreat and regrowth phase. In both cases, mass losses through basal melt and discharge (iceberg calving) practically vanish for temperatures above 8 °C of warming, when the ice sheet no longer has contact with the ocean (during retreat) or is not yet in contact with the ocean (during regrowth) and basal melt from grounded ice is negligible. The majority of net mass loss during retreat occurs between 6 °C and 10 °C of warming—caused mainly by the surface elevation feedback in East Antarctica—whereas most of the mass gain during regrowth happens at lower temperatures of 2–5 °C of warming (resulting in a 'flatter' distribution in the phase space of total mass flux versus warming). This is expected: in order for ice to form, temperatures must first cool considerably, because the snowline first has to descend down to the ice-free bedrock surface.

Discussion and conclusion

Our analysis reveals a strong, multi-step hysteresis behaviour of the Antarctic Ice Sheet, confirming that in certain regions ice loss is in fact irreversible even if temperatures were to return to colder levels. We focus here solely on the ice-internal feedbacks; however, it should be noted that additional feedback mechanisms such as the ice–albedo feedback, as well as, for instance, sea-level changes due to the effect of self-gravitation or due to a large amount of meltwater added to the ocean, could further dampen or amplify the ice sheet's response to sustained warming. One such positive feedback in the ice–ocean

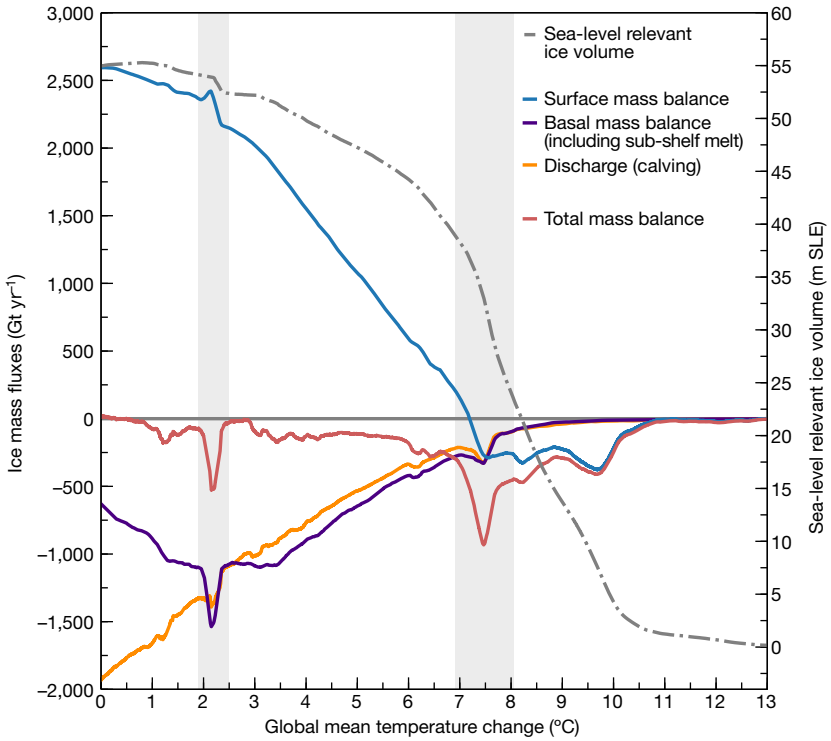

Fig. 5 | Ocean-driven versus atmosphere-driven ice loss. Antarctic ice mass fluxes (in gigatonnes per year) showing the contributions of different atmospheric and oceanic processes to the total ice mass changes over the entire range of GMT anomalies along the upper hysteresis branch derived from the quasi-static reference simulation. Positive flux values denote mass gains; negative values denote mass losses. The vertical grey bars mark the locations of the two major temperature thresholds described in the text, which are associated with sharp drops in the total mass balance. The sea-level relevant ice-sheet volume (in m SLE) is indicated by the dashed grey line with respect to the right-hand axis.

interaction, which might lead to warm waters being trapped below the sea surface, recently received renewed attention[47].

Another potential positive feedback process, termed the marine ice-cliff instability, has only lately been brought to wider attention[25]. Underpinned by observations of rapid ice-shelf and glacier retreat it has been suggested that hydrofracturing might lead to high coastal ice cliffs that become mechanically unstable at heights exceeding 90 m above the waterline, eventually causing the disintegration of marine ice sheets[48]. However, this effect is still disputed[49,50] and is not considered in the simulations presented here.

Although our approach encompasses the dominant processes and feedbacks relevant for studying the long-term response of the Antarctic Ice Sheet, fully interactive ice–atmosphere–ocean simulations are required to project the Antarctic ice evolution under future emission trajectories. In reality, temperatures have been changing and will probably continue to change at much faster rates than considered here. Our results should thus not be confused with sea-level projections—we deliberately choose small forcing rates here because this allows us to identify critical temperature thresholds decisive for the overall stability of the Antarctic Ice Sheet. Our results imply that, if the Paris Agreement to limit global warming to well below 2 °C above pre-industrial temperatures is not met, one or more critical thresholds might be subsequently crossed in Antarctica, committing us to long-term, possibly irreversible, sea-level rise of up to dozens of metres.[51,52]

Online content

Any methods, additional references, Nature Research reporting summaries, source data, extended data, supplementary information, acknowledgements, peer review information; details of author contributions and competing interests; and statements of data and code availability are available at https://doi.org/10.1038/s41586-020-2727-5.

1. Fretwell, P. et al. Bedmap2: improved ice bed, surface and thickness datasets for Antarctica. *Cryosphere* **7**, 375–393 (2013).
2. Turney, C. S. M. et al. Early Last Interglacial ocean warming drove substantial ice mass loss from Antarctica. *Proc. Natl Acad. Sci. USA* **117**, 3996–4006 (2020).
3. Bueler, E. & Brown, J. Shallow shelf approximation as a 'sliding law' in a thermomechanically coupled ice sheet model. *J. Geophys. Res.* **114**, F03008 (2009).
4. Winkelmann, R. et al. The Potsdam Parallel Ice Sheet Model (PISM-PIK)—Part 1: Model description. *Cryosphere* **5**, 715–726 (2011).
5. *PISM, a Parallel Ice Sheet Model: User's Manual* http://pism-docs.org/ (2017).
6. The IMBIE Team. Mass balance of the Antarctic Ice Sheet from 1992 to 2017. *Nature* **558**, 219–222 (2018).
7. Rignot, E. et al. Four decades of Antarctic Ice Sheet mass balance from 1979–2017. *Proc. Natl Acad. Sci. USA* **116**, 1095–1103 (2019).
8. Intergovernmental Panel on Climate Change (IPCC) *Climate Change 2013: The Physical Science Basis. Contribution of Working Group I to the Fifth Assessment Report of the Intergovernmental Panel on Climate Change* (Cambridge Univ. Press, 2013).
9. Frieler, K. et al. Consistent evidence of increasing Antarctic accumulation with warming. *Nat. Clim. Chang.* **5**, 348–352 (2015).
10. Winkelmann, R., Levermann, A., Martin, M. A. & Frieler, K. Increased future ice discharge from Antarctica owing to higher snowfall. *Nature* **492**, 239–242 (2012).
11. Weertman, J. Stability of ice-age ice sheets. *J. Geophys. Res.* **66**, 3783–3792 (1961).
12. Oerlemans, J. Some basic experiments with a vertically-integrated ice-sheet model. *Tellus* **33**, 1–11 (1981).
13. Huybrechts, P. et al. Response of the Greenland and Antarctic ice sheets to multi-millennial greenhouse warming in the Earth system model of intermediate complexity LOVECLIM. *Surv. Geophys.* **32**, 397–416 (2011).
14. Levermann, A. & Winkelmann, R. A simple equation for the melt elevation feedback of ice sheets. *Cryosphere* **10**, 1799–1807 (2016).
15. Clarke, G. K. C., Nitsan, U. & Paterson, W. S. B. Strain heating and creep instability in glaciers and ice sheets. *Rev. Geophys.* **15**, 235–247 (1977).
16. Weertman, J. Stability of the junction of an ice sheet and an ice shelf. *J. Glaciol.* **13**, 3–11 (1974).
17. Mercer, J. H. West Antarctic ice sheet and CO_2 greenhouse effect: a threat of disaster. *Nature* **271**, 321–325 (1978).
18. Gudmundsson, G. H., Krug, J., Durand, G., Favier, L. & Gagliardini, O. The stability of grounding lines on retrograde slopes. *Cryosphere* **6**, 1497–1505 (2012).
19. Gomez, N., Pollard, D. & Holland, D. Sea-level feedback lowers projections of future Antarctic Ice-Sheet mass loss. *Nat. Commun.* **6**, 8798 (2015).
20. Fyke, J., Sergienko, O., Löfverström, M., Price, S. F. & Lenaerts, J. T. M. An overview of interactions and feedbacks between ice sheets and the Earth system. *Rev. Geophys.* **56**, 361–408 (2018).

21. Golledge, N. R. et al. The multi-millennial Antarctic commitment to future sea-level rise. *Nature* **526**, 421–425 (2015).
22. Winkelmann, R., Levermann, A., Ridgwell, A. & Caldeira, K. Combustion of available fossil fuel resources sufficient to eliminate the Antarctic Ice Sheet. *Sci. Adv.* **1**, e1500589 (2015).
23. Robinson, A., Calov, R. & Ganopolski, A. Multistability and critical thresholds of the Greenland ice sheet. *Nat. Clim. Chang.* **2**, 429–432 (2012).
24. Huybrechts, P. Formation and disintegration of the Antarctic ice sheet. *Ann. Glaciol.* **20**, 336–340 (1994).
25. DeConto, R. M. & Pollard, D. Contribution of Antarctica to past and future sea-level rise. *Nature* **531**, 591–597 (2016).
26. Sutter, J., Gierz, P., Grosfeld, K., Thoma, M. & Lohmann, G. Ocean temperature thresholds for Last Interglacial West Antarctic Ice Sheet collapse. *Geophys. Res. Lett.* **43**, 2675–2682 (2016).
27. Golledge, N. R., Levy, R. H., McKay, R. M. & Naish, T. R. East Antarctic ice sheet most vulnerable to Weddell Sea warming. *Geophys. Res. Lett.* **44**, 2343–2351 (2017).
28. Pattyn, F. et al. The Greenland and Antarctic ice sheets under 1.5 °C global warming. *Nat. Clim. Chang.* **8**, 1053–1061 (2018).
29. Pollard, D. & DeConto, R. M. Modelling West Antarctic ice sheet growth and collapse through the past five million years. *Nature* **458**, 329–332 (2009).
30. Alley, R. B. et al. Oceanic forcing of ice-sheet retreat: West Antarctica and more. *Annu. Rev. Earth Planet. Sci.* **43**, 207–231 (2015).
31. Dutton, A. et al. Sea-level rise due to polar ice-sheet mass loss during past warm periods. *Science* **349**, aaa4019 (2015).
32. Pollard, D. & DeConto, R. M. Hysteresis in Cenozoic Antarctic ice-sheet variations. *Glob. Planet. Change* **45**, 9–21 (2005).
33. Gasson, E. G. W., DeConto, R. M., Pollard, D. & Levy, R. Dynamic Antarctic ice sheet during the early to mid-Miocene. *Proc. Natl Acad. Sci. USA* **113**, 3459–3464 (2016).
34. Liu, Z. et al. Global cooling during the Eocene-Oligocene climate transition. *Science* **323**, 1187–1190 (2009).
35. Hansen, J., Sato, M., Russell, G. & Kharecha, P. Climate sensitivity, sea level and atmospheric carbon dioxide. *Phil. Trans. R. Soc. A* **371**, 20120294 (2013).
36. Rahmstorf, S. & England, M. H. Influence of Southern Hemisphere winds on North Atlantic Deep Water flow. *J. Phys. Oceanogr.* **27**, 2040–2054 (1997).
37. Albrecht, T., Winkelmann, R. & Levermann, A. Glacial-cycle simulations of the Antarctic Ice Sheet with the Parallel Ice Sheet Model (PISM)—Part 1: Boundary conditions and climatic forcing. *Cryosphere* **14**, 599–632 (2020).
38. Schmidtko, S., Heywood, K. J., Thompson, A. F. & Aoki, S. Multidecadal warming of Antarctic waters. *Science* **346**, 1227–1231 (2014).
39. Mouginot, J., Rignot, E. & Scheuchl, B. Sustained increase in ice discharge from the Amundsen Sea Embayment, West Antarctica, from 1973 to 2013. *Geophys. Res. Lett.* **41**, 1576–1584 (2014).
40. Rignot, E., Mouginot, J., Morlighem, M., Seroussi, H. & Scheuchl, B. Widespread, rapid grounding line retreat of Pine Island, Thwaites, Smith, and Kohler glaciers, West Antarctica, from 1992 to 2011. *Geophys. Res. Lett.* **41**, 3502–3509 (2014).
41. Favier, L. et al. Retreat of Pine Island Glacier controlled by marine ice-sheet instability. *Nat. Clim. Chang.* **4**, 117–121 (2014).
42. Joughin, I., Smith, B. E. & Medley, B. Marine ice sheet collapse potentially under way for the Thwaites Glacier Basin, West Antarctica. *Science* **344**, 735–738 (2014).
43. Naish, T. R. et al. Obliquity-paced Pliocene West Antarctic ice sheet oscillations. *Nature* **458**, 322–328 (2009).
44. Levermann, A. et al. The multimillennial sea-level commitment of global warming. *Proc. Natl Acad. Sci. USA* **110**, 13745–13750 (2013).
45. Mengel, M. & Levermann, A. Ice plug prevents irreversible discharge from East Antarctica. *Nat. Clim. Chang.* **4**, 451–455 (2014).
46. Golledge, N. R. et al. Antarctic climate and ice-sheet configuration during the early Pliocene interglacial at 4.23 Ma. *Clim. Past* **13**, 959–975 (2017).
47. Golledge, N. R. et al. Global environmental consequences of twenty-first-century ice-sheet melt. *Nature* **566**, 65–72 (2019).
48. Bassis, J. N. & Walker, C. C. Upper and lower limits on the stability of calving glaciers from the yield strength envelope of ice. *Proc. R. Soc. A* **468**, 913–931 (2012).
49. Edwards, T. L. et al. Revisiting Antarctic ice loss due to marine ice-cliff instability. *Nature* **566**, 58–64 (2019).
50. Meredith, M. et al. Polar regions. In *IPCC Special Report on the Ocean and Cryosphere in a Changing Climate* (eds Pörtner, H.-O. et al.) https://www.ipcc.ch/srocc/chapter/chapter-3-2/ (in the press).
51. Schellnhuber, H. J., Rahmstorf, S. & Winkelmann, R. Why the right climate target was agreed in Paris. *Nat. Clim. Chang.* **6**, 649–653 (2016).
52. Lenton, T. M. et al. Climate tipping points—too risky to bet against. *Nature* **575**, 592–595 (2019).

Methods

Ice-sheet model

We use a modified version of the Parallel Ice Sheet Model (PISM) release v1.0, an open-source, three-dimensional, thermo-mechanically coupled ice-sheet/ice-shelf model[3–5]. Running in hybrid mode, PISM combines equations of the shallow-ice approximation and shallow-shelf (or shelfy-stream) approximation (SSA) of the Stokes flow over the entire ice-sheet/ice-shelf domain. Superimposing the shallow-ice approximation and SSA velocity solutions enables a consistent transition of stress regimes across the grounded-ice to floating-ice boundary[4]. The ice rheology is based on the Glen–Paterson–Budd–Lliboutry–Duval flow law[53] with Glen exponent $n = 3$.

Basal shear stress in the vicinity of the grounding line is computed at subgrid scale using a linear interpolation of the height above buoyancy between adjacent grounded and floating cells[54]. Melt rates at the shelf base are not interpolated across the grounding line.

Basal sliding and subglacial hydrology

In PISM, basal sliding is parameterized based on a generalized power-law formulation[55]:

$$\boldsymbol{\tau}_b = -\tau_c \frac{\mathbf{u}_b}{u_{th}^q |\mathbf{u}_b|^{1-q}},$$

where $\boldsymbol{\tau}_b$ is the basal shear stress, $\mathbf{u}_b$ is the basal sliding velocity, τ_c is the yield stress (see below) and u_{th} is a threshold velocity, chosen here to be 100 m yr^{-1}. Depending on the sliding exponent $0 \le q \le 1$, this 'pseudo-plastic' approach spans a wide range from purely plastic Coulomb sliding ($q = 0$) to sliding in which basal velocity and basal shear stress are linearly related ($q = 1$). In our simulations we use a sliding exponent of $q = 0.75$.

The yield stress τ_c is determined as a function of till material properties and of the effective till pressure N_{till}, using the Mohr–Coulomb criterion[56]:

$$\tau_c = \tan\phi N_{till},$$

where ϕ is called the till friction angle, a heuristic shear strength parameter for the till material property, which is optimized iteratively in the grounded-ice region such that the mismatch of equilibrium and modern surface elevation is minimized[37].

To determine the effective pressure on the till, the modelled amount of water in the till layer W_{till} is used. Meltwater generated in the subglacial layer is stored locally in the till up to a thickness of saturated substrate of $W_{till}^{max} = 2$ m. The hydrology parameterization is non-conserving in the sense that additional water above this maximum thickness is lost permanently.

With the effective water thickness of the till layer $s = W_{till}/W_{till}^{max}$ and the ice overburden pressure P_0, N_{till} is parameterized as in ref. [57]:

$$N_{till} = \min\left\{P_0, N_0\left(\frac{\delta P_0}{N_0}\right)^s 10^{(e_0/C_c)(1-s)}\right\}$$

For the constant parameters N_0, e_0 and C_c, we use the values adopted from ref. [57]. For saturated till ($s = 1$) we find $N_{till}^{min} = \delta P_0$, where δ is a certain fraction of the overburden (here set to 4%), at which the till reaches maximum capacity and excess water will be drained. We note that the effective till pressure cannot exceed the overburden pressure, that is, $N_{till}^{max} = P_0$.

Glacial isostatic adjustment

Changes in the elevation of the bed topography due to changes in ice load are modelled using a sophisticated Earth-deformation model based on refs. [58,59]. It consists of a purely elastic plate lithosphere overlying a linearly viscous half-space (of viscosity $\eta = 1 \times 10^{21}$ Pa s and density $\rho = 3{,}300$ kg m^{-3}) that represents the upper mantle (see figure 3 in ref. [58]). The half-space model utilizes a time-dependent partial differential equation, which generalizes and improves upon the widely used Elastic Lithosphere Relaxing Asthenosphere (ELRA) model[59]. This allows for computationally inexpensive calculations based on fast Fourier transforms. A further advantage of this formulation is that the relaxation time of the bed elevation is not considered a constant, instead, relaxation times are mode-dependent, thus closely approximating the approach used within more complex GIA models. As in our simulations typical ice-dynamical timescales are much longer than those of the elastic part of the Earth model (which are of the order of magnitude of 10^1 years), we applied only the viscous part.

Surface mass balance

Mean annual and mean summer surface air temperatures are parameterized based on multiple regression analysis of ERA-Interim data[60], as a function of latitude and surface elevation, using an atmospheric lapse rate Γ of −8.2 °C km^{-1} (ref. [37]). For surface accumulation we use the 1986–2005 mean precipitation from the output of the Regional Atmospheric Climate MOdel (RACMOv2.3p2; ref. [61]). As a modification from PISM release v1.0, we introduce a climatic correction for precipitation P based on the difference between ice-model surface elevation and the interpolated elevation in the climate model or observational dataset. The base precipitation pattern P_0 is now scaled exponentially with model ice surface elevation change Δh, using an exponential factor of 41% per kilometre of elevation change, similar to the approach followed by ref. [25]:

$$P = P_0 \times \exp(\gamma \Delta h),$$

where

$$\gamma = 5\%^\circ\mathrm{C}^{-1} \times \Gamma$$

Thereby, the factor γ accounts for a 5% change in accumulation per degree of atmospheric temperature change[9], assuming a linear relationship between these two quantities. For consistency reasons, the exponential correction of precipitation is also used for the applied temperature anomaly forcing using the same γ.

Ice surface melt and runoff are computed using a positive degree-day (PDD) scheme, with melt coefficients of 3 mm per PDD for snow and 9 mm per PDD for ice, respectively, and also accounting for natural variability using a 5 °C standard deviation.

Sub-shelf melting

Sub-shelf melt rates are computed using the Potsdam Ice-shelf Cavity mOdel (PICO; ref. [62]). PICO extends the ocean box model approach by ref. [63], simulating the vertical overturning circulation in ice-shelf cavities, thus enabling the computation of sub-shelf melt rates consistent with this circulation. It mimics the exchange with ocean water masses in front of the ice shelves, which is physically based on the 'ice-pump' mechanism, using parameters for overturning strength and turbulent heat exchange of 0.5×10^6 m^6 s^{-1} kg^{-1} and 1×10^{-5} m s^{-1}, respectively.

Calving

Iceberg calving at the ice-shelf margin is calculated from principal strain rates[64]. In this 'eigencalving' approach, the average calving rate is proportional to the product of principal components of the horizontal strain rates derived from SSA velocities at the shelf front. The proportionality factor is set to be 1×10^{17} m s. Additionally, we apply a minimum thickness criterion of 50 m (PISM default) at the calving front, based on the observation that ice-shelf calving fronts commonly have a minimum thickness and appear to be unstable below that[65]. Ice shelves are also removed in all areas which were 'open ocean' during the initial

timestep. The two latter calving conditions are mainly imposed due to numerical reasons, but show almost no influence on the ice volume, in particular during the regrowth phase (Extended Data Fig. 4b).

Ice-sheet reference state

To define appropriate ice-sheet initial conditions for our experiments, we generate the required equilibrium state under climatic boundary conditions from the available data from the second half of the twentieth century. Since the Antarctic Ice Sheet has experienced notable changes during the past decades owing to anthropogenic climate change, much larger than the natural variability experienced over most of the Holocene[66], we interpret the pre-industrial ice-sheet configuration as the closest analogue to this equilibrium state. Temperature anomalies are therefore taken with respect to pre-industrial levels in all experiments presented here.

The equilibrium state is a slightly modified version of an equilibrium state generated as part of the initial state intercomparison exercise (initMIP-Antarctica; ref. [67]), the latest set of experiments of the Ice Sheet Model Intercomparison Project for CMIP6 (ISMIP6), which is the primary Coupled Model Intercomparison Project Phase 6 (CMIP6) activity focusing on the Greenland and Antarctic ice sheets. The initMIP equilibrium simulation was initialized from Bedmap2 geometry[1], with surface mass balance from RACMOv2.3p2 1986–2005 mean[61] and observed values of ocean temperature and salinity at the sea floor on the continental shelf, averaged over the period 1975–2012 (ref. [38]), to drive PICO (for more details, see appendix B12 of ref. [67]).

Using the initMIP equilibrium as input, we extend the simulation for another 150 kyr with our version of PISM. Main model modifications relate to the bedrock now being allowed to deform under changing ice-sheet geometry as well as the parameterization of the surface air temperature in the atmosphere module, now being based on multiple regression analysis of ERA-Interim data, from which the surface melt is calculated via the above-described PDD scheme.

All simulations were performed on a regular rectangular grid with 16 km horizontal resolution. The vertical grid is quadratically spaced, ranging between 20 m at the ice base and 100 m at the top of the thickest ice domes. The simulations shown in Extended Data Fig. 4g use a horizontal grid resolution of 8 km and a vertical grid spacing ranging from 13 m at the ice base to 87 m at the upper ice surface.

Climate and ocean inputs and forcings

To study the long-term response of the Antarctic Ice Sheet to changing global temperatures, we trace the ice sheet's hysteresis with respect to temperature changes with an approach based on section 2b of ref. [36]. In this approach, a spatially uniform temperature anomaly that is gradually changing over time is applied to the boundary climate in the model. The rate of warming is slower than the typical response timescale of the ice sheet. This ensures that the system can follow the change, remaining as close as possible to equilibrium at all times, while taking into account computational constraints. Our simulation is initialized using the ice-sheet reference state described above and then the incrementally increasing temperature anomaly is applied until complete deglaciation is achieved. To trace the lower branch of the hysteresis, the temperature anomaly is then incrementally decreased again, starting from the bare bedrock, until the ice sheet is regrown to its initial extent. Different warming rates have been tested (0.001 °C yr^{-1}, 0.0005 °C yr^{-1}, 0.0002 °C yr^{-1} and 0.0001 °C yr^{-1}). The rate of change of GMT anomaly used here to derive the quasi-static reference hysteresis diagram (blue curve in Fig. 2) is 0.0001 °C yr^{-1}. At every full degree, as well as every half degree between 6 °C and 9 °C of warming on the upper branch, we further extend the simulations at fixed temperatures until the ice sheet fully reaches a steady state, that is, volume changes become negligible.

To translate the global mean surface air temperature anomaly into regional atmospheric and oceanic temperature changes, the GMT anomalies are scaled using constant scaling factors. In a long-term simulation with the coupled climate model ECHAM5/MPIOM (https://mpimet.mpg.de/en/science/models/mpi-esm) it has been shown that the ratios between the GMT and the near-surface air temperature and ocean temperature at about 400 m depth in the region south of 66 °S are almost constant on long timescales[68]. In these simulations the scaling factors approach values of 1.8 and 0.7 with respect to GMT for the regional near-surface air temperature and the ocean temperature, respectively (section 4.3 of ref. [37]).

Sensitivity ensemble

An ensemble of model sensitivity simulations was carried out to verify the robustness of the presented findings with respect to changes in various critical model parameters. These include the horizontal grid resolution, the maximum allowed extent for ice-shelf calving, the viscous response of the upper mantle to ice loading, ice-stream sliding, and the SSA ice-flow enhancement factor[4]. The results of the sensitivity ensemble are shown in Extended Data Fig. 4.

Data availability

All data used for this study are publicly available. Antarctic surface mass balance data from RACMO2.3p2 were downloaded from https://www.projects.science.uu.nl/iceclimate/publications/data/2018/index.php#vwessem2018_tc. Antarctic bedrock topography and ice thickness data are from the Bedmap2 compilation, available at https://secure.antarctica.ac.uk/data/bedmap2/. The Schmidtko ocean temperature and salinity dataset can be retrieved at https://www.geomar.de/en/staff/fb1/po/sschmidtko/southern-ocean/. The datasets generated and analysed during this study are available from the corresponding author upon reasonable request.

Code availability

PISM is freely available as open-source code from https://github.com/pism/pism. The code version used in this study is available at https://doi.org/10.5281/zenodo.3956431. PISM input data are pre-processed using https://github.com/pism/pism-ais with original data citations.

53. Lliboutry, L. A. & Duval, P. Various isotropic and anisotropic ices found in glaciers and polar ice caps and their corresponding rheologies. *Ann. Geophys.* **3**, 207–224 (1985).
54. Feldmann, J., Albrecht, T., Khroulev, C., Pattyn, F. & Levermann, A. Resolution-dependent performance of grounding line motion in a shallow model compared with a full-Stokes model according to the MISMIP3d intercomparison. *J. Glaciol.* **60**, 353–360 (2014).
55. Schoof, C. & Hindmarsh, R. C. A. Thin-film flows with wall slip: an asymptotic analysis of higher order glacier flow models. *Q. J. Mech. Appl. Math.* **63**, 73–114 (2010).
56. Cuffey, K. M. & Paterson, W. S. B. *The Physics of Glaciers* 4th edn (Elsevier, Academic Press, 2010).
57. Bueler, E. & van Pelt, W. Mass-conserving subglacial hydrology in the Parallel Ice Sheet Model version 0.6. *Geosci. Model Dev.* **8**, 1613–1635 (2015).
58. Lingle, C. S. & Clark, J. A. A numerical model of interactions between a marine ice-sheet and the solid Earth: application to a West Antarctic ice stream. *J. Geophys. Res. Oceans* **90**, 1100–1114 (1985).
59. Bueler, E., Lingle, C. S. & Brown, J. Fast computation of a viscoelastic deformable Earth model for ice-sheet simulations. *Ann. Glaciol.* **46**, 97–105 (2007).
60. Dee, D. P. et al. The ERA-Interim reanalysis: configuration and performance of the data assimilation system. *Q. J. R. Meteorol. Soc.* **137**, 553–597 (2011).
61. van Wessem, J. M. et al. Modelling the climate and surface mass balance of polar ice sheets using RACMO2—Part 2: Antarctica (1979–2016). *Cryosphere* **12**, 1479–1498 (2018).
62. Reese, R., Albrecht, T., Mengel, M., Asay-Davis, X. & Winkelmann, R. Antarctic sub-shelf melt rates via PICO. *Cryosphere* **12**, 1969–1985 (2018).
63. Olbers, D. & Hellmer, H. A box model of circulation and melting in ice shelf caverns. *Ocean Dyn.* **60**, 141–153 (2010).
64. Levermann, A. et al. Kinematic first-order calving law implies potential for abrupt ice-shelf retreat. *Cryosphere* **6**, 273–286 (2012).
65. Albrecht, T., Martin, M. A., Haseloff, M., Winkelmann, R. & Levermann, A. Parameterization for subgrid-scale motion of ice-shelf calving fronts. *Cryosphere* **5**, 35–44 (2011).
66. Cuffey, K. M. et al. Deglacial temperature history of West Antarctica. *Proc. Natl Acad. Sci. USA* **113**, 14249–14254 (2016).
67. Seroussi, H. et al. initMIP-Antarctica: an ice sheet model initialization experiment of ISMIP6. *Cryosphere* **13**, 1441–1471 (2019).
68. Li, C., von Storch, J.-S. & Marotzke, J. Deep-ocean heat uptake and equilibrium climate response. *Clim. Dyn.* **40**, 1071–1086 (2013).
69. Rignot, E., Mouginot, J. & Scheuchl, B. Ice flow of the Antarctic Ice Sheet. *Science* **333**, 1427–1430 (2011).

Acknowledgements J.G., J.F.D. and R.W. were supported by the Leibniz Association project DominoES. T.A. and R.W. are supported by the Deutsche Forschungsgemeinschaft (DFG) in the framework of the priority program "Antarctic Research with comparative investigations in Arctic ice areas" by grants WI4556/2-1 and WI4556/4-1, and within the framework of the PalMod project (FKZ: 01LP1925D) supported by the German Federal Ministry of Education and Research (BMBF) as a Research for Sustainability initiative (FONA). J.F.D. is grateful for financial support by the Stordalen Foundation via the Planetary Boundary Research Network (PB.net), the Earth League's EarthDoc programme, and the European Research Council Advanced Grant project ERA (Earth Resilience in the Anthropocene; grant ERC-2016-ADG-743080). This research was supported by the European Union's Horizon 2020 research and innovation programme under grant agreement number 820575 (TiPACCs). The development of PISM is supported by NASA grant NNX17AG65G and NSF grants PLR-1603799 and PLR-1644277. We further acknowledge the European Regional Development Fund (ERDF), the German Federal Ministry of Education and Research (BMBF) and the Land Brandenburg for supporting this project by providing resources on the high-performance computer system at the Potsdam Institute for Climate Impact Research. We thank M. Mengel for providing the Antarctic equilibrium used as a basis for the simulations.

Author contributions R.W. conceived the study. All authors designed the research and contributed to the analysis. J.G. carried out the model simulations. J.G. and R.W. wrote the manuscript with contributions from all co-authors.

Competing interests The authors declare no competing interests.

Additional information

Supplementary information is available for this paper at https://doi.org/10.1038/s41586-020-2727-5.

Correspondence and requests for materials should be addressed to R.W.

Peer review information *Nature* thanks Nicholas R Golledge and the other, anonymous, reviewer(s) for their contribution to the peer review of this work.

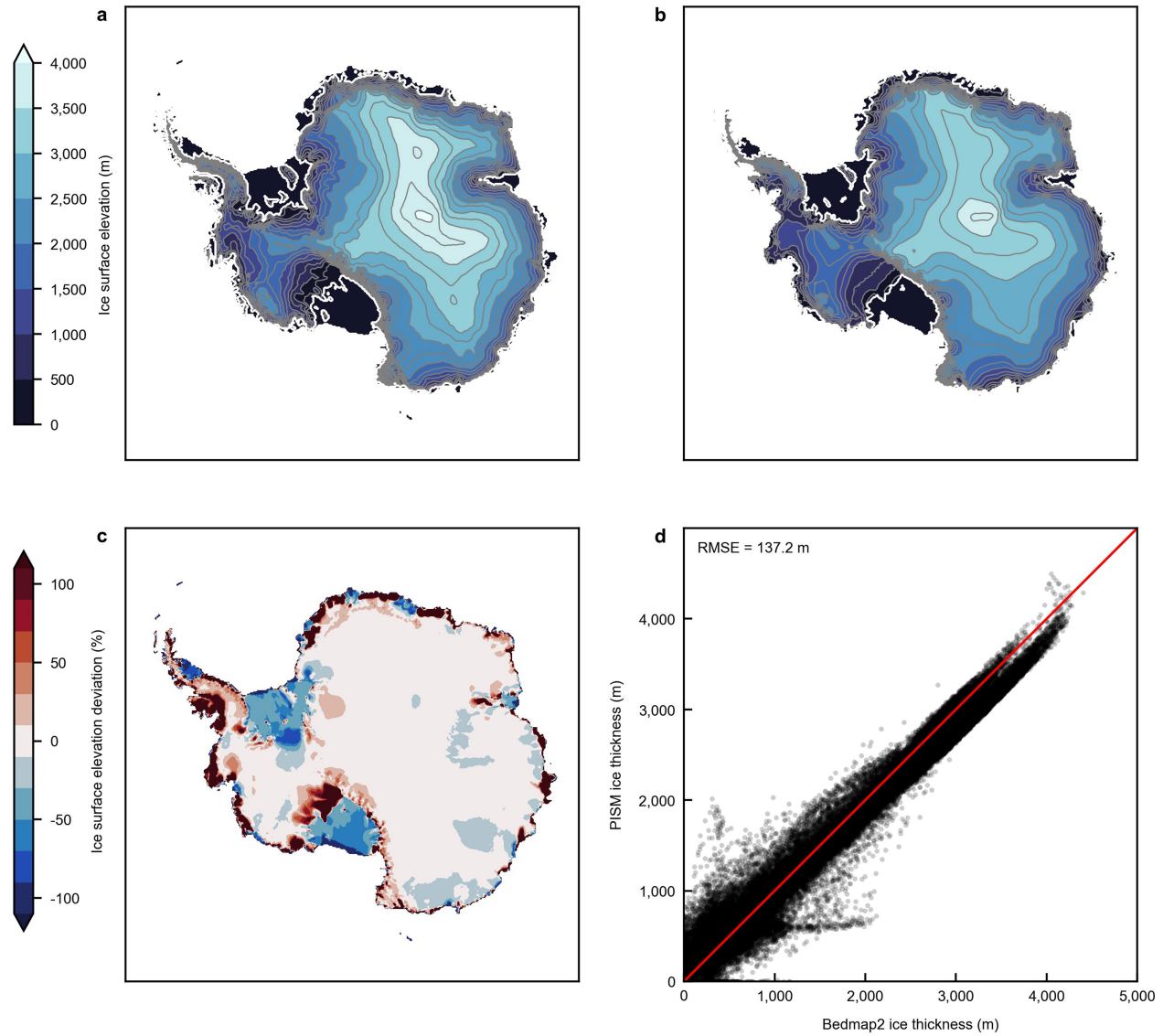

Extended Data Fig. 1 | Comparison of modelled and observed ice geometry. **a**, Observed ice surface elevation (Bedmap2, ref. [1]), regridded to 16 km. Grounding lines are shown in white; surface-height contours are given every 250 m. **b**, Modelled ice surface elevation of the reference state serving as initial configuration for the hysteresis experiments. Grounding lines are shown in white; surface-height contours are given every 250 m. **c**, Modelled minus observed (Bedmap2) ice surface elevation. **d**, Scatter plot for comparison of modelled and observed ice thickness for each grid cell. Red identity line illustrates where modelled ice thickness would perfectly match the observations. RMSE, root-mean-square error.

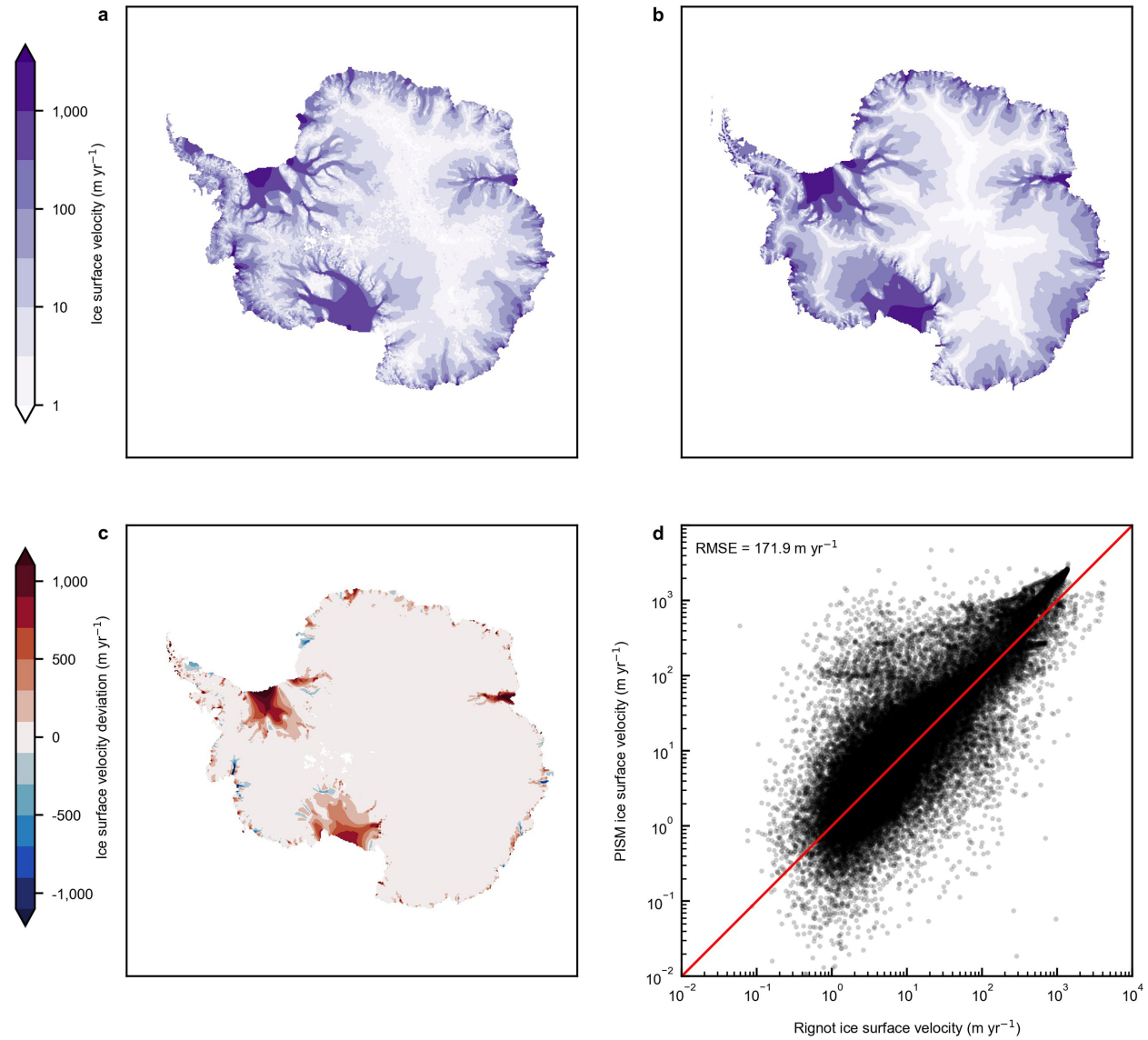

Extended Data Fig. 2 | Comparison of modelled and observed ice velocities. **a**, Observed ice surface velocities[69], regridded to 16 km. **b**, Modelled ice surface velocities of reference state. **c**, Model minus observed ice surface velocity. **d**, Scatter plot of model versus observed ice surface velocity. The red line is the identity line.

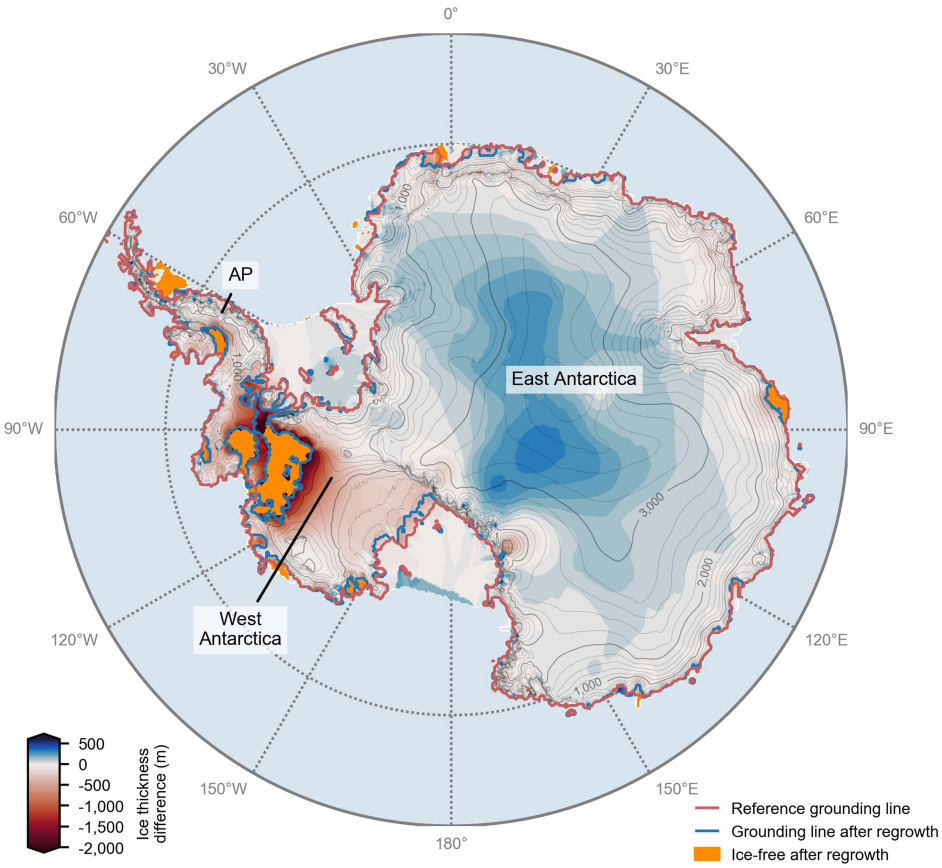

Extended Data Fig. 3 | Regrown Antarctica. Equilibrium ice thickness difference of the regrown ice-sheet configuration (at pre-industrial temperatures, that is, 0 °C GMT anomaly) minus the reference ice-sheet thickness. Red lines denote the reference grounding-line locations; blue lines show their respective locations after regrowth. Areas of the ice sheet which do not regrow to their original extents are highlighted in orange. Surface-height contour lines of the regrown ice sheet are given at 200-m intervals.

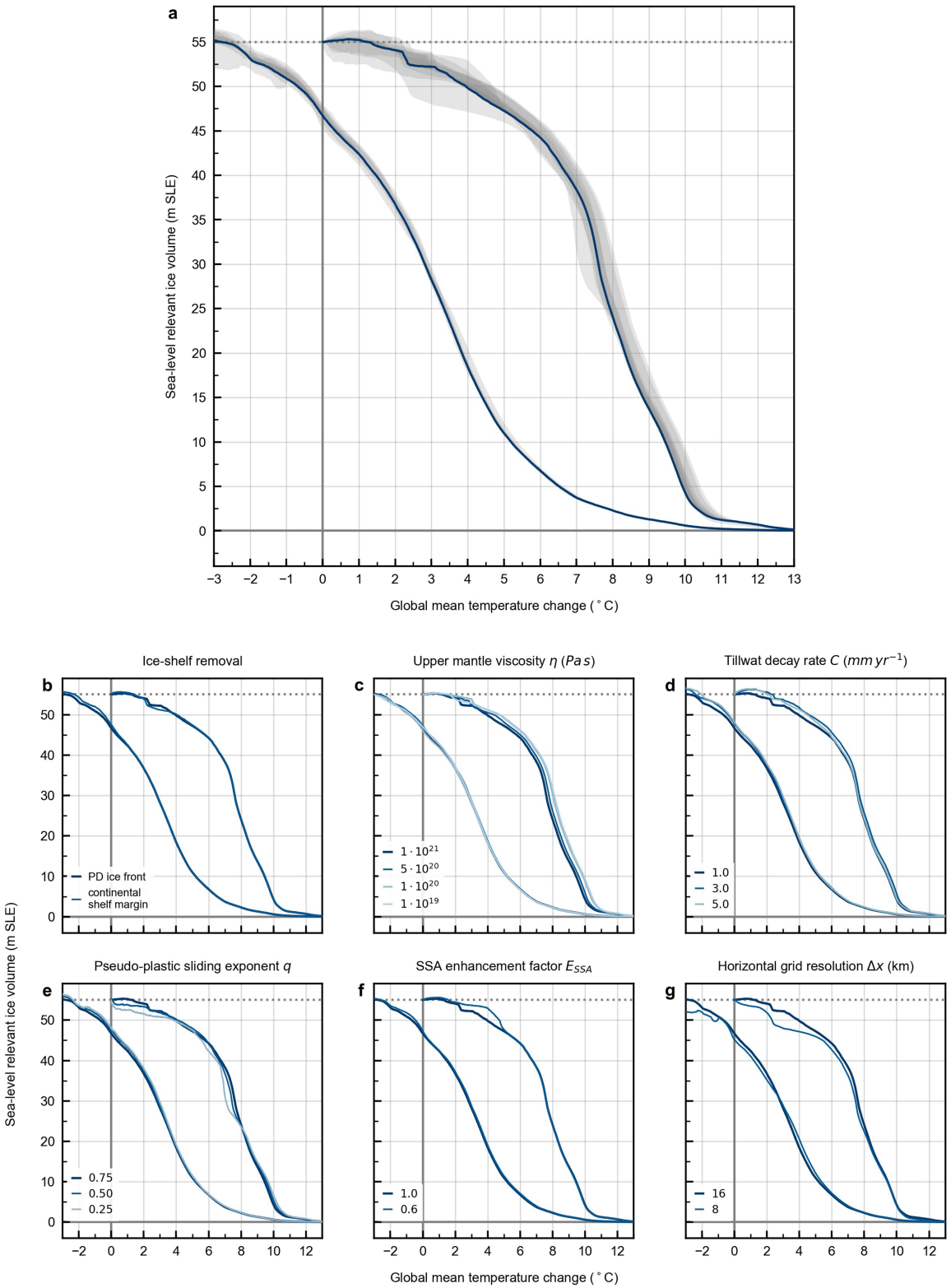

Extended Data Fig. 4 | Hysteresis sensitivity to model parameter variations. **a**, Sea-level relevant ice volume for a global warming rate of 1 °C per 10,000 years above pre-industrial conditions. The blue curve is the same as the blue curve in Fig. 2; the grey shadings show the model sensitivity by encompassing the total range of individual model responses with respect to the variation of critical model parameters, as detailed below. **b**–**g**, Same as **a**, but showing the respective simulations for the tested model parameters (thin blue lines) in comparison to the reference simulation (thick blue line): **b**, ice-shelf removal mechanism (PD, present-day); **c**, viscosity of the upper mantle in the Earth-deformation model; **d**, decay rate of the subglacial meltwater in the till layer; **e**, unitless exponent in the 'pseudo-plastic' sliding law; **f**, unitless flow enhancement factor for the SSA velocities[4]; and **g**, horizontal model grid resolution.

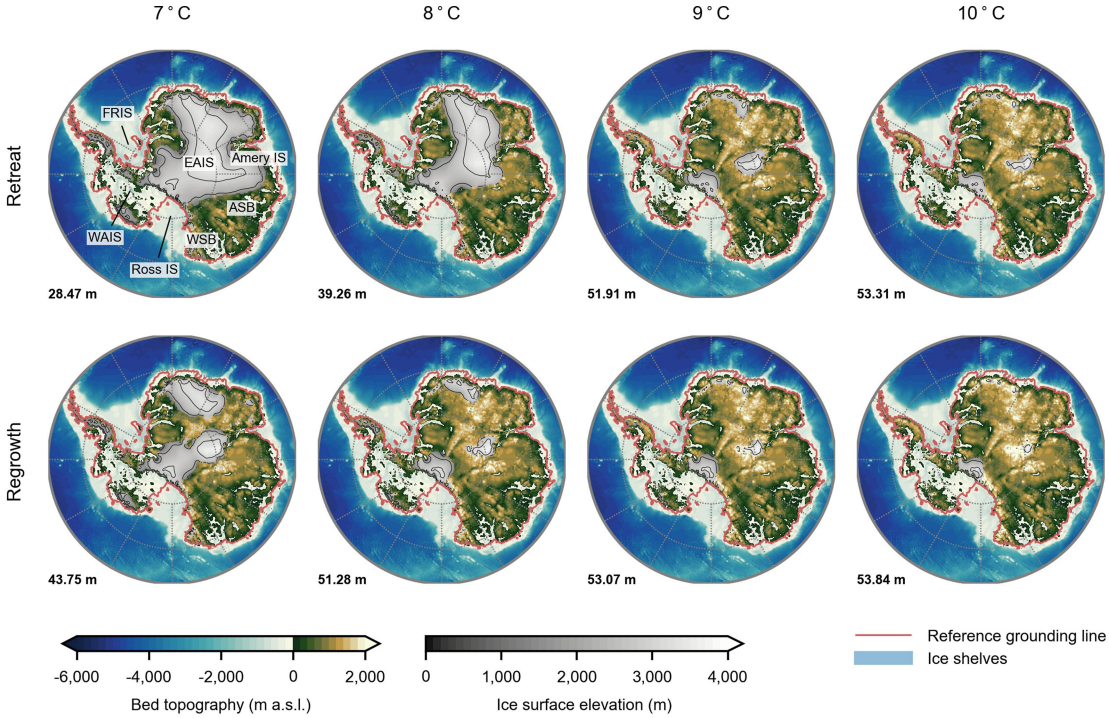

Extended Data Fig. 5 | Long-term ice loss for different warming levels. This figure continues Fig. 4; the equilibrium ice-sheet surface elevation is shown in metres for different warming levels (7 °C, 8 °C, 9 °C and 10 °C GMT anomaly above pre-industrial level), comparing the retreat (upper panels) and regrowth (lower panels) branch of the hysteresis curve. Ice surface-height contours are delineated at 1,000-m intervals. Grounding-line locations of the reference state are shown in red; ice shelves are marked in light blue. The absolute sea-level relevant ice-volume anomaly compared to the reference state (in m SLE), that is, the committed sea-level rise, is given for each panel. Blue shadings illustrate the bedrock depth in metres below the present-day sea level; brown shadings illustrate the bedrock elevation in metres above the present-day sea level (a.s.l.). ASB, Aurora subglacial basin; WSB, Wilkes subglacial basin.

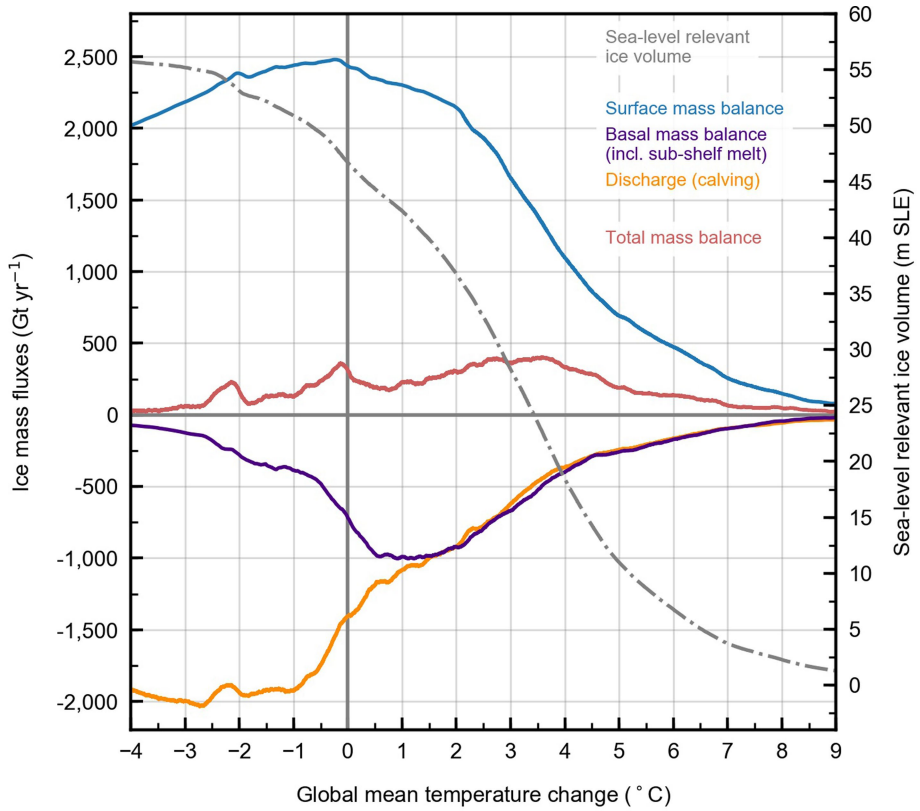

Extended Data Fig. 6 | Ocean-driven versus atmosphere-driven ice loss (regrowth branch). Antarctic ice mass fluxes showing (in gigatonnes per year) the contributions of different atmospheric and oceanic processes to the total ice mass changes over the entire range of GMT anomalies along the lower hysteresis branch derived from the quasi-static reference simulation. Positive flux values denote mass gains, negative values denote mass losses. The sea-level relevant ice-sheet volume (in m SLE) is indicated by the dashed grey line with respect to the right-hand axis.